

Deep Historical Borrowing Framework to Prospectively and Simultaneously Synthesize Control Information in Confirmatory Clinical Trials with Multiple Endpoints

Tianyu Zhan^{1,†}, Yiwang Zhou², Ziqian Geng¹, Yihua Gu¹, Jian Kang³,
Li Wang¹, Xiaohong Huang¹ and Elizabeth H. Slate⁴

¹ Data and Statistical Sciences, AbbVie Inc., North Chicago, IL, USA

² Department of Biostatistics, St. Jude Children's Research Hospital, Memphis, TN, USA

³ Department of Biostatistics, University of Michigan, Ann Arbor, MI, USA

⁴ Department of Statistics, Florida State University, Tallahassee, FL, USA

[†] Corresponding author: Tianyu Zhan, 1 Waukegan Road, North Chicago, IL 60064, USA.

tianyu.zhan.stats@gmail.com

Abstract

In current clinical trial development, historical information is receiving more attention as it provides utility beyond sample size calculation. Meta-analytic-predictive (MAP) priors and robust MAP priors have been proposed for prospectively borrowing historical data on a single endpoint. To simultaneously synthesize control information from multiple endpoints in confirmatory clinical trials, we propose to approximate posterior probabilities from a Bayesian hierarchical model and estimate critical values by deep learning to construct pre-specified strategies for hypothesis testing. This feature is important to ensure study integrity by establishing prospective decision functions before the trial conduct. Simulations are performed to show that our method properly controls family-wise

error rate (FWER) and preserves power as compared with a typical practice of choosing constant critical values given a subset of null space. Satisfactory performance under prior-data conflict is also demonstrated. We further illustrate our method using a case study in Immunology.

Keywords: Bayesian hierarchical model; Deep learning; Family-wise error rate control; Power preservation; Prospective algorithm

1 Introduction

Historical control data are usually summarized as estimates of parameters needed to calculate the sample size when designing a traditional Phase III randomized clinical trial (Chow et al., 2007). This relevant information can be properly borrowed for the current trial to make it more efficient and ethical by allowing fewer patients randomized to the control group or decreasing the total sample size (Berry et al., 2010; Viele et al., 2014). Some challenges exist in applying this framework to clinical trials, especially confirmatory studies. While it is always possible to *retrospectively* use historical information once the new evidence is available, it is appealing to ensure study integrity by designing a *prospective* algorithm for leveraging historical data (Neuenschwander et al., 2010). Moving beyond the “sweet spot” where the borrowed information and the current data are similar, one needs to properly discount historical information to control the bias and the type I error rates (Viele et al., 2014).

In the context of a single endpoint, Neuenschwander et al. (2010) proposed a novel meta-analytic-predictive (MAP) approach to prospectively borrow historical information for the current trial. Schmidli et al. (2014) further developed an innovative method to approximate the MAP prior by a mixture of conjugate priors, and therefore the posterior distribution is available in a closed form. A robust MAP prior is then formulated by adding a weakly informative component to discount historical data under prior-data conflict (Schmidli et al., 2014). Moving further to confirmatory clinical trials, most use multiple endpoints to assess the effects of the study drug (Food and Drug Administration, 2017). A Bayesian hierarchical model is a natural approach to simultaneously synthesize information from multiple endpoints (Berry et al., 2010). However, taking a trial with binary endpoints as an example, additional non-trivial work is needed to generalize the MAP framework to

approximate the joint prior of response rates and to investigate whether the resulting multivariate posterior distribution is available analytically.

As an alternative, we propose a two-stage Deep Neural Networks (DNN) guided algorithm to build pre-specified decision functions before initiation of the current trial. It takes advantage of the strong functional representation of DNN (Goodfellow et al., 2016; Bach, 2017; Yarotsky, 2017) to directly approximate posterior probabilities in Section 3.2, and critical values in Section 3.3. Our proposed method has several appealing features. First, it is a prospective approach in the sense that pre-trained DNN models can be locked in files before initiation of the current trial to ensure study integrity. Moreover, our method provides an accurate type I error rate control by modeling corresponding critical values. As an alternative, simulation-based type I error control by using constant critical values within a subset of the null space can be viewed as a “worst case scenario” adjustment, which leads to power loss when the type I error rate is conservative (Proschan and Hunsberger, 1995; Graf et al., 2014; Zhan et al., 2020b). More demonstration is provided in Section 4. Additionally, simulations and the case study show that our method has relatively small bias and mean squared error (MSE) under prior-data conflict by properly discounting prior information.

The remainder of this article is organized as follows. In Section 2, we introduce a Bayesian hierarchical model on control data from several historical studies. Next we propose DNN-based algorithms to approximate the posterior probabilities and critical values to build pre-specified decision functions for hypothesis testing in Section 3. Simulations in Section 4 and a case study in Section 5 are conducted to evaluate the performance of our method. Concluding remarks are provided in Section 6.

2 A Bayesian hierarchical model on historical control data

Consider a two-group randomized controlled clinical trial with I ($I \geq 2$) endpoints to study the efficacy of a treatment versus placebo. We consider a setup of $I = 2$ binary endpoints for illustration, but our method can be readily generalized to $I > 2$ endpoints and other types of endpoints. Denote $R_{i,0}^{(t)}$ as the number of responders in the current treatment group for endpoint i , where $i \in \{1, \dots, I\}$, and $n_0^{(t)}$ as the total number of subjects from the treatment arm in the current trial. The superscript

“(t)” denotes the treatment group. For each endpoint i , a Beta conjugate prior is assumed on the Binomial sampling distribution with rate $\psi_{i,0}^{(t)}$,

$$R_{i,0}^{(t)} \mid \psi_{i,0}^{(t)} \sim \text{Binomial} \{n_0^{(t)}, \psi_{i,0}^{(t)}\}, \quad \psi_{i,0}^{(t)} \sim \text{Beta}(a_i, b_i), \quad i = 1, \dots, I. \quad (1)$$

The control data are available in the current trial and J historical studies. The corresponding notations are denoted as $R_{i,j}^{(c)}$ and $n_j^{(c)}$, where $j = 0$ indicates the current trial, $j \in \{1, \dots, J\}$ is the index of historical study j , and $i \in \{1, \dots, I\}$ refers to endpoint i . We consider the following Bayesian hierarchical model on the control data (Neuenschwander et al., 2010; Schmidli et al., 2014),

$$R_{i,j}^{(c)} \mid \psi_{i,j}^{(c)} \sim \text{Binomial} \{n_j^{(c)}, \psi_{i,j}^{(c)}\}, \quad \mu_{i,j} = \text{logit} \{ \psi_{i,j}^{(c)} \}, \quad \boldsymbol{\mu}_j \sim \text{MVN}(\boldsymbol{\theta}, \Sigma), \quad (2)$$

where $\boldsymbol{\mu}_j = (\mu_{1,j}, \dots, \mu_{I,j})$, for $i \in \{1, \dots, I\}$, $j \in \{0, 1, \dots, J\}$, and $\text{MVN}(\boldsymbol{\theta}, \Sigma)$ denotes a multivariate Normal distribution with mean vector $\boldsymbol{\theta}$ and variance-covariance matrix Σ . A vague prior is assumed on $\boldsymbol{\theta}$, and an *InverseWishart* (Σ_0, k) prior is assigned to the variance-covariance matrix Σ with positive definite $I \times I$ matrix Σ_0 and degrees of freedom $k \geq I$. The expectation of a *Wishart* (Σ_0, k) is $k(\Sigma_0)^{-1}$, and therefore Σ_0/k is a prior guess for Σ . We use $\mathbf{D}_H = [R_{i,j}^{(c)}, n_j^{(c)}, i \in \{1, \dots, I\}, j \in \{1, \dots, J\}]$ to denote control information in J historical studies, and $\mathbf{D}_N = [R_{i,0}^{(c)}, n_0^{(c)}, R_{i,0}^{(t)}, n_0^{(t)}, i \in \{1, \dots, I\}]$ as data in the current new trial.

Our quantity of interest is the posterior probability of observing a promising treatment effect in the current trial,

$$S_i = \text{Pr} \{ \psi_{i,0}^{(t)} - \psi_{i,0}^{(c)} > \theta_i \mid \mathbf{D}_H, \mathbf{D}_N \}, \quad i = 1, \dots, I, \quad (3)$$

where θ_i is a pre-specified constant for endpoint i . The decision function of rejecting the null hypothesis pertaining to endpoint i is if $S_i > \tilde{c}_i$. The critical value \tilde{c}_i can be interpreted as a threshold to claim a significant treatment effect in the i th endpoint with controlled type I error rates. The computation of \tilde{c}_i is studied in the next section to control the family-wise error rate (FWER) at a nominal level α . We denote $\mathbf{S} = (S_1, \dots, S_I)$ as a vector of those posterior probabilities.

Since the posterior probabilities \mathbf{S} in (3) usually do not have closed forms, we estimate them empirically by a large number of Monte Carlo samples. Specifically, posterior samples $\psi_{i,0}^{(t)}$ are simulated

from the conjugate prior model in (1), and posterior samples $\psi_{i,0}^{(c)}$ in the Bayesian hierarchical model (2) are obtained by the Markov chain Monte Carlo (MCMC) method based on current trial data (Berry et al., 2010). However, it is appealing to build a prospective algorithm before conducting the current new trial to ensure the study integrity. In studies with a single binary endpoint ($I = 1$), Schmidli et al. (2014) proposed a novel approach by approximating the Meta Analytic Predictive (MAP) prior $p\{\psi_{i,0}^{(c)}|\mathbf{D}_H\}$ with a mixture of Beta distributions, and hence the posterior distribution $p\{\psi_{i,0}^{(c)}|\mathbf{D}_H, \mathbf{D}_N\}$ becomes a weighted average of Beta distributions. In the context of multiple endpoints ($I \geq 2$), a Bayesian hierarchical model in (2) is a natural approach to simultaneously synthesize control information (Berry et al., 2010). Even if one can utilize several base distributions to approximate the multivariate prior $p\{\boldsymbol{\psi}_0^{(c)}|\mathbf{D}_H\}$, where $\boldsymbol{\psi}_0^{(c)} = \{\psi_{1,0}^{(c)}, \dots, \psi_{I,0}^{(c)}\}$, the joint posterior probability \mathbf{S} does not necessarily have an analytic closed form.

As an alternative, we propose to directly approximate \mathbf{S} based on observed historical data \mathbf{D}_H and varying simulated new trial data \mathbf{D}_N by deep neural networks (DNN) in the study design stage. After collecting results from the current trial, one can instantly compute \mathbf{S} and conduct downstream hypothesis testing based on pre-specified approximation functions.

3 A DNN-based historical borrowing framework

In this section, we first provide a short review on DNN in Section 3.1, and then introduce our DNN guided historical borrowing framework by directly approximating the posterior probabilities and posterior means in Section 3.2. In Section 3.3, we further estimate corresponding critical values by DNNs to control FWER in the strong sense. The hypothesis testing based on observed current trial data is discussed in Section 3.4.

3.1 Review of DNN

Deep learning is a specific subfield of machine learning as a new take on learning representations from data with successive layers (Chollet and Allaire, 2018). A major application of Deep Neural Networks (DNN) is to approximate some functions with input data (Goodfellow et al., 2016). DNN defines a mapping function $F(\mathbf{M}; \boldsymbol{\phi})$ that learns the value of parameters $\boldsymbol{\phi}$ that result in the best

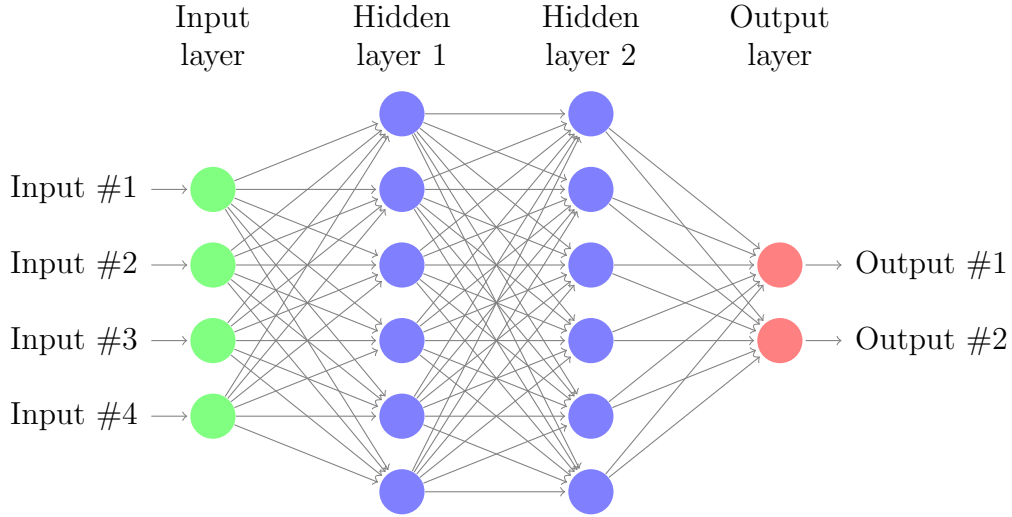


Figure 1: A Deep Neural Network with two hidden layers.

function approximation of output \mathbf{S} based on input data \mathbf{M} , where ϕ denotes a stack of all weights and bias parameters in the DNN. To simply notations, we use \mathbf{S} in (3) to denote the output, because later on DNN is utilized to approximate this posterior probability. For example in Figure 1, the left input \mathbf{M} of dimension 4 is transferred by 2 hidden layers to approximate a 2-dimensional output \mathbf{S} on the right.

Typically, training a DNN involves the following four components: layers, input data and corresponding output, loss function, and optimizer (Chollet and Allaire, 2018). To avoid the potential over-fitting, cross-validation is commonly used to select the architecture from a pool of candidates (Goodfellow et al., 2016). The loss function measures how well the fitted DNN $F(\mathbf{M}; \hat{\phi})$ approximates the output \mathbf{S} . The mean squared error (MSE) loss can be utilized if \mathbf{S} is continuous. The optimizer determines how the network will be updated based on the loss function. It usually implements a specific variant of the stochastic gradient descent (SGD) algorithm; for example, RMSProp (Hinton et al., 2012) has been shown to be an effective and practical optimization algorithm for DNN (Goodfellow et al., 2016), and is used in this article.

3.2 Posterior probabilities approximation

We denote $\mathbf{R}_i^{(c)} = \{R_{i,1}^{(c)}, \dots, R_{i,J}^{(c)}\}$ as a stack of numbers of responders in all historical studies J for endpoint i , $i = 1, \dots, I$, and further denote $\mathbf{R}_H^{(c)} = \{\mathbf{R}_1^{(c)}, \dots, \mathbf{R}_I^{(c)}\}$. Corresponding notations are $\mathbf{R}_N^{(c)} = \{R_{1,0}^{(c)}, \dots, R_{I,0}^{(c)}\}$ for the current control group, and $\mathbf{R}_N^{(t)} = \{R_{1,0}^{(t)}, \dots, R_{I,0}^{(t)}\}$ for the current

treatment arm. The subscript “H” refers to historical data, while “N” corresponds to new trial data. We consider $\mathcal{P}_i^{(c)}$ as a parameter space covering $\psi_{i,j}^{(c)}$ for endpoint i in all J historical studies and $\psi_{i,0}^{(c)}$ in the current study. For example, $\mathcal{P}_i^{(c)} = \{\psi_i^{(c)} : \psi_i^{(c)} \in (0.1, 0.5)\}$ indicates that the control response rate for endpoint i in all historical studies and the current study ranges from 0.1 to 0.5. It can be set wider as needed. Similarly, \mathcal{T}_i is the parameter space of the treatment effect Δ_i for endpoint i .

In Algorithm 1, we utilize DNN to construct a mapping function $F_S(\mathbf{M}; \widehat{\phi})$ to approximate \mathbf{S} in (3) based on input data \mathbf{M} , where $\mathbf{M} = \{\mathbf{R}_N^{(c)}, \mathbf{R}_N^{(t)}\}$ and $\widehat{\phi}$ are the estimated parameters in DNN. Note that DNN is utilized to estimate the quantity \mathbf{S} instead of the posterior distribution. We consider a setup where sample size $\{n_0^{(c)}, n_1^{(c)}, \dots, n_J^{(c)}, n_0^{(t)}\}$ and historical data $\mathbf{R}_H^{(c)}$ are constants. Therefore, the simulated input data $\mathbf{M} = \{\mathbf{R}_N^{(c)}, \mathbf{R}_N^{(t)}\}$ for DNN only contains the number of responders in the current trial. When there are $I = 2$ endpoints, \mathbf{M} has 4 elements and \mathbf{S} has 2 elements as shown in Figure 1. One can build a more general DNN function to accommodate varying sample size and varying historical data. In Step 1, \mathbf{M} and \mathbf{R} are based on simulated current trial data before the current trial conduct. Their counterparts $\widetilde{\mathbf{M}}$ and $\widetilde{\mathbf{R}}$ from observed current trial data are plugged in the trained $F_S(\mathbf{M}; \widehat{\phi})$ to estimate \mathbf{S} at Section 3.4.

In Step 2, we perform cross-validation with 80% as the training data and the remaining 20% as the validation data to select a proper DNN structure and other hyperparameters (Goodfellow et al., 2016). By increasing the number of hidden layers H_l , the number of nodes H_n in DNN and the number of training epochs H_e , the empirical MSE from the training dataset usually decreases, but the validation MSE may increase. We then apply regulation approaches to increase the generalizability of the model while keeping the training MSE below a certain tolerance, say 10^{-3} . The regulation approaches include the dropout technique which randomly sets a number of nodes as zeros during training with a dropout rate H_d , and the mini-batch approach which stochastically selects a small batch of data with batch size H_b in computing the gradient in the optimization algorithm. Several structures around this sub-optimal structure are added to the candidate pool for cross-validation (Goodfellow et al., 2016; Zhan et al., 2020a). The final DNN structure is selected as the one with the smallest validation error and is utilized in Step 3 to obtain the estimated posterior probability $\widehat{\mathbf{S}}$ by $\widehat{\mathbf{S}} = F_S(\mathbf{M}; \widehat{\phi})$. This selected structure is also used for DNN F_P introduced next and for DNNs to estimate critical values in the next section. One can implement this structure selection process

when training other DNNs. Since output \mathbf{S} is continuous, we use the MSE loss in training the DNN. The estimated posterior probability $\widehat{\mathbf{S}}$ is further truncated within 0 and 1. The same loss function is used for approximating posterior means of control response rates and for approximating critical values discussed later. On the implementation of DNN, interested readers can refer to Chollet and Allaire (2018) and our shared R code with link provided in the Supplementary Materials for more details.

Similarly, we train another DNN $F_P [\mathbf{R}_N^{(c)}; \widehat{\phi}_P]$ to approximate the posterior means of control response rates $[\psi_{1,0}^{(c)}, \dots, \psi_{I,0}^{(c)}]$. Only the simulated numbers of control responders $\mathbf{R}_N^{(c)}$ are included as input data for DNN F_P , because the treatment and control group are assumed to be independent by models (1) and (2). Other training details are the same with the DNN F_S introduced in the previous paragraph.

Here we provide some remarks on accommodating correlations between endpoints in the Step 1 of simulating training data. Per model (2), given response rate $\psi_{i,j}^{(c)}$, the number of responders $R_{i,j}^{(c)}$ are independent between endpoints. The correlation is captured by the variance-covariance matrix Σ in the multivariate Normal distribution of $\boldsymbol{\mu}_j$. In Step 1, even though we uniformly draw $\psi_{i,0}^{(c)}$ from its support $\mathcal{P}_i^{(c)}$, we can capture a broad range of correlations on response rates by simulating a sufficiently large number B of training data. In Step 3, the DNN F_S learns the functional form of mapping \mathbf{M} to \mathbf{S} with correlations accounted. Therefore, we do not directly simulate correlated endpoints in Step 1, but cover varying magnitudes of correlations on response rates in DNN training. In practice, one should check validation error and operating characteristics in testing to make sure that the size B is large enough. An alternative but more complicated approach is to simulate correlated rates $\psi_{i,j}^{(c)}$ with several varying correlation coefficients to reduce training data size B .

3.3 FWER control in the strong sense

In this section, we discuss how to compute the critical value \tilde{c}_i in the decision rule $S_i > \tilde{c}_i$ of rejecting the null hypothesis pertaining to endpoint i to strongly control FWER at a nominal level α .

Family-wise error rate (FWER) is the probability of rejecting at least one true null hypothesis. FWER is said to be controlled at level α in the strong sense if it does not exceed α under any configuration of true and false hypotheses (Bretz et al., 2016). Define H_1 and H_2 as the single null

Algorithm 1 Train a DNN $F_S(\mathbf{M}; \widehat{\phi})$ to approximate the posterior distributions \mathbf{S} based on simulated \mathbf{M}

1. Construct a training dataset for the DNN of size B . In each training data b , uniformly draw $\psi_{i,0}^{(c)}$ from $\mathcal{P}_i^{(c)}$, $\Delta_{i,0}$ from \mathcal{T}_i and set $\psi_{i,0}^{(t)} = \psi_{i,0}^{(c)} + \Delta_{i,0}$, for $i = 1, \dots, I$. The training input data $\mathbf{M} = [\mathbf{R}_N^{(c)}, \mathbf{R}_N^{(t)}]$ is further simulated from Binomial distributions with their corresponding response rates. The output \mathbf{S} in (3) is computed based on simulated \mathbf{M} , fixed sample sizes $\{n_0^{(c)}, n_1^{(c)}, \dots, n_J^{(c)}, n_0^{(t)}\}$ and observed historical data $\mathbf{R}_H^{(c)}$ as demonstrated in Section 2.
 2. Perform cross-validation on several candidate DNN structures to select one with the smallest validation error for final training.
 3. Train a DNN to build an approximating function $\widehat{\mathbf{S}} = F_S(\mathbf{M}; \widehat{\phi})$ to estimate \mathbf{S} based on simulated \mathbf{M} , where $\widehat{\phi}$ are the estimated parameters in DNN.
-

hypotheses where only endpoint 1 or 2 has no treatment effect, and H_{12} as the global null hypothesis where neither endpoint has treatment effects. In the context of $I = 2$ endpoints, we need to control the following three erroneous probabilities,

$$Pr\{S_1 > c_1 \mid H_1\} \leq \alpha, \quad H_1 : \psi_{1,0}^{(c)} = \psi_{1,0}^{(t)}, \psi_{2,0}^{(c)} < \psi_{2,0}^{(t)} \quad (4)$$

$$Pr\{S_2 > c_2 \mid H_2\} \leq \alpha, \quad H_2 : \psi_{2,0}^{(c)} = \psi_{2,0}^{(t)}, \psi_{1,0}^{(c)} < \psi_{1,0}^{(t)} \quad (5)$$

$$Pr\{(S_1 > c_{12}) \cup (S_2 > c_{12}) \mid H_{12}\} \leq \alpha, \quad H_{12} : \psi_{1,0}^{(c)} = \psi_{1,0}^{(t)}, \psi_{2,0}^{(c)} = \psi_{2,0}^{(t)} \quad (6)$$

where c_1 is the critical value to control error rate under H_1 , c_2 for H_2 , and c_{12} for H_{12} .

In Algorithm 2, we train three DNNs to estimate these three critical values: c_1 , c_2 and c_{12} . Taking H_1 in (4) as an example, we define $\psi_{1,0}^{(c,t)}$ as the common value of $\psi_{1,0}^{(c)}$ and $\psi_{1,0}^{(t)}$ under H_1 . The training input data is denoted as $\mathbf{M}_1 = \{\psi_{1,0}^{(c,t)}, \psi_{2,0}^{(c)}, \Delta_{2,0}\}$, which is simulated before the current trial conduct. In Step 1, we simulate B_1 varying \mathbf{M}_1 's from parameter spaces to get the training input data. Given each training feature \mathbf{M}_1 , we then simulate B'_1 samples under H_1 and compute their estimated posterior probabilities at $\widehat{\mathbf{S}} = F_S(\mathbf{M}; \widehat{\phi})$ based on the DNN F_S obtained from Algorithm 1. The critical value c_1 is empirically calculated as the upper α quantile of \widehat{S}_1 in $\widehat{\mathbf{S}}$ to satisfy (4). We further train a DNN to obtain a mapping function $\widehat{c}_1 = F_1(\mathbf{M}_1; \widehat{\phi}_1)$ to approximate c_1 based on simulated \mathbf{M}_1 . Step 2 constructs $\widehat{c}_2 = F_2(\mathbf{M}_2; \widehat{\phi}_2)$ under H_2 in (5), and Step 3 computes $\widehat{c}_{12} = F_{12}(\mathbf{M}_{12}; \widehat{\phi}_{12})$ under H_{12} in (6). Similar to Algorithm 1 at Section 3.2, Algorithm 2 is also pre-specified before the current trial conduct in the sense that \mathbf{M}_1 , \mathbf{M}_2 , \mathbf{M}_{12} are simulated response rates. Other training

details are the same with Section 3.2.

3.4 Hypothesis testing based on observed current trial data

After conducting Algorithm 1 in Section 3.2 and Algorithm 2 in Section 3.3 based on simulated current trial data, one can save well-trained DNNs in files to ensure the integrity of the current trial conduct. In this section, we illustrate how to perform hypothesis testing based on $\widetilde{\mathbf{R}}_N^{(c)} = \{\widetilde{R}_{1,0}^{(c)}, \widetilde{R}_{2,0}^{(c)}\}$ as the observed number of responder in the current control group, and $\widetilde{\mathbf{R}}_N^{(t)} = \{\widetilde{R}_{1,0}^{(t)}, \widetilde{R}_{2,0}^{(t)}\}$ in the current treatment group.

The first step is estimate posterior probabilities $\widehat{\mathbf{S}} = F_S(\widetilde{\mathbf{M}}; \widehat{\boldsymbol{\phi}})$ with the DNN F_S obtained in Algorithm 1, where $\widetilde{\mathbf{M}} = \{\widetilde{\mathbf{R}}_N^{(c)}, \widetilde{\mathbf{R}}_N^{(t)}\}$. The next step is to calculate critical values based on three trained DNNs obtained in Algorithm 2. Taking H_1 as an example, we denote $\widetilde{\mathbf{M}}_1 = \left[\left\{ \frac{\widetilde{R}_{1,0}^{(c)} + \widetilde{R}_{1,0}^{(t)}}{n_0^{(c)} + n_0^{(t)}}, \frac{\widetilde{R}_{2,0}^{(c)}}{n_0^{(c)}}, \frac{\widetilde{R}_{2,0}^{(t)}}{n_0^{(t)}} - \frac{\widetilde{R}_{2,0}^{(c)}}{n_0^{(c)}} \right\} \right]$ as the empirical estimator of $\mathbf{M}_1 = \{\psi_{1,0}^{(c,t)}, \psi_{2,0}^{(c)}, \Delta_{2,0}\}$. We then estimate its critical value at $\widehat{c}_1 = F_1(\widetilde{\mathbf{M}}_1; \widehat{\boldsymbol{\phi}}_1)$ based on the trained DNN F_1 . Correspondingly, we estimate c_2 under H_2 at $\widehat{c}_2 = F_2(\widetilde{\mathbf{M}}_2; \widehat{\boldsymbol{\phi}}_2)$, where $\widetilde{\mathbf{M}}_2 = \left[\frac{\widetilde{R}_{1,0}^{(c)}}{n_0^{(c)}}, \frac{\widetilde{R}_{1,0}^{(t)}}{n_0^{(t)}} - \frac{\widetilde{R}_{1,0}^{(c)}}{n_0^{(c)}}, \left\{ \frac{\widetilde{R}_{2,0}^{(c)} + \widetilde{R}_{2,0}^{(t)}}{n_0^{(c)} + n_0^{(t)}} \right\} \right]$, and estimate c_{12} under H_{12} at $\widehat{c}_{12} = F_{12}(\widetilde{\mathbf{M}}_{12}; \widehat{\boldsymbol{\phi}}_{12})$, where $\widetilde{\mathbf{M}}_{12} = \left[\left\{ \frac{\widetilde{R}_{1,0}^{(c)} + \widetilde{R}_{1,0}^{(t)}}{n_0^{(c)} + n_0^{(t)}}, \left\{ \frac{\widetilde{R}_{2,0}^{(c)} + \widetilde{R}_{2,0}^{(t)}}{n_0^{(c)} + n_0^{(t)}} \right\} \right]$.

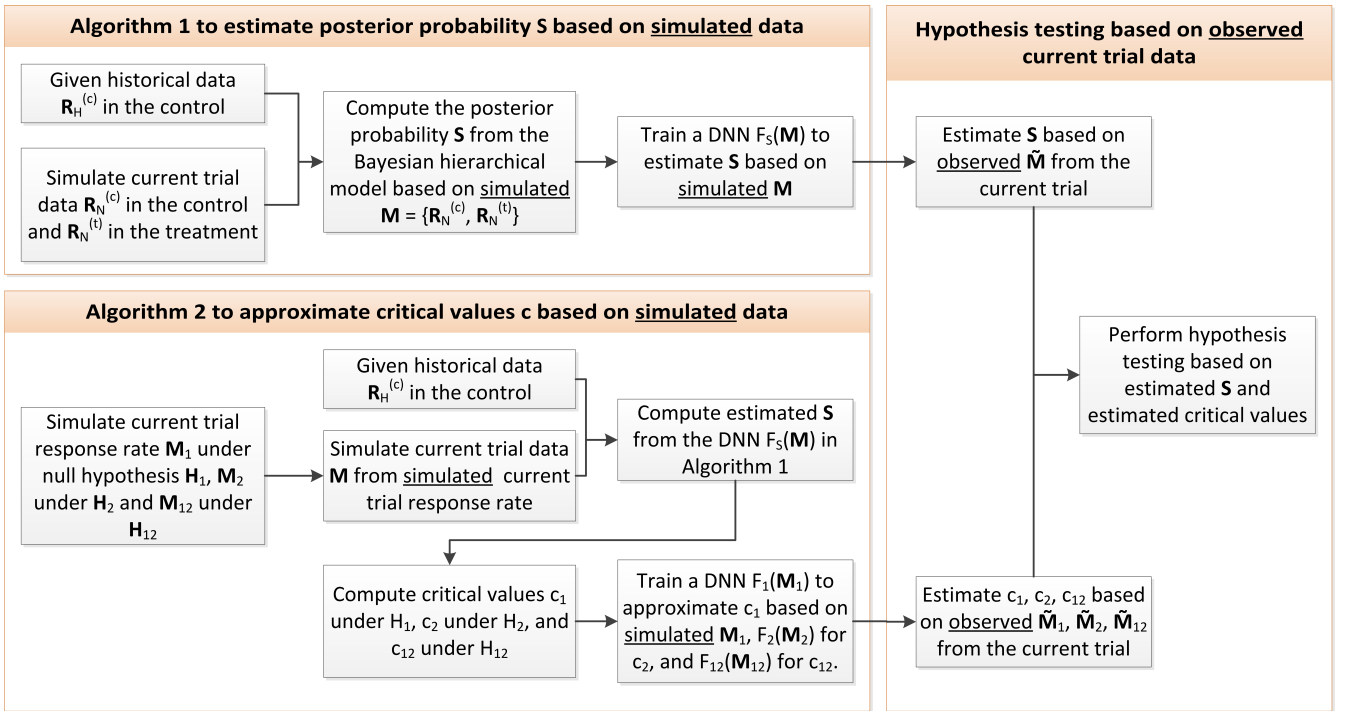
Now we are ready to perform hypothesis testing on treatment effects based on estimated posterior probabilities $\widehat{\mathbf{S}} = \{\widehat{S}_1, \widehat{S}_2\}$, and estimated critical values \widehat{c}_1 , \widehat{c}_2 and \widehat{c}_{12} . Since the strong control of FWER is under all configurations of true and false null hypotheses specified in (4), (5) and (6), we set $\widetilde{c}_1 = \max(\widehat{c}_1, \widehat{c}_{12})$ for rejecting null hypothesis H_1 with the decision function $\widehat{S}_1 > \widetilde{c}_1$, and correspondingly $\widetilde{c}_2 = \max(\widehat{c}_2, \widehat{c}_{12})$ for H_2 . This is analogous to the closure principle of handling multiplicity issues, where the rejection of a particular elementary hypothesis requires the rejection of all intersection hypotheses containing it (Tamhane and Gou, 2018).

In Figure 2, we provide a flowchart to illustrate the role of Algorithms 1 and 2 based on simulated current trial data, and hypothesis testing based on observed current trial data.

Algorithm 2 Train three DNNs to approximate critical values based on simulated \mathbf{M}_1 , \mathbf{M}_2 and \mathbf{M}_{12}

1. Under H_1 in (4), simulate training input data $\mathbf{M}_1 = \{\psi_{1,0}^{(c,t)}, \psi_{2,0}^{(c)}, \Delta_{2,0}\}$ under H_1 of size B_1 . Given each training response rate \mathbf{M}_1 , simulate B'_1 sets of responders \mathbf{M} and compute their estimated posterior probabilities at $\hat{\mathbf{S}} = F_S(\mathbf{M}; \hat{\phi})$ based on the DNN F_S from Algorithm 1. The critical value c_1 is computed as the upper α quantile of \hat{S}_1 in $\hat{\mathbf{S}}$. Train a DNN to obtain the mapping function $\hat{c}_1 = F_1(\mathbf{M}_1; \hat{\phi}_1)$.
 2. Under H_2 in (5), train another DNN $\hat{c}_2 = F_2(\mathbf{M}_2; \hat{\phi}_2)$ to estimate c_2 based on $\mathbf{M}_2 = \{\psi_{1,0}^{(c)}, \Delta_{1,0}, \psi_{2,0}^{(c,t)}\}$ of training data size B_2 and null data size B'_2 .
 3. Under H_{12} in (6), the training input data is $\mathbf{M}_{12} = \{\psi_{1,0}^{(c,t)}, \psi_{2,0}^{(c,t)}\}$. The critical value c_{12} is computed by solving a non-linear equation in (6) based on \hat{S}_1 and \hat{S}_2 of size B'_{12} . The fitted DNN is denoted as $\hat{c}_{12} = F_{12}(\mathbf{M}_{12}; \hat{\phi}_{12})$.
-

Figure 2: Flowchart of Algorithm 1 and 2 and hypothesis testing. Algorithm 1 utilizes DNN to approximate posterior probability S in (3) based on simulated current trial data. Algorithm 2 trains DNN to estimate critical values c to control type I error rates based on simulated data from null hypothesis. The hypothesis testing is based on observed current trial data.



4 Simulation studies

In this section, we conduct simulation studies to evaluate the performance of our proposed method, and compare it with the Meta-Analytic-Prior (MAP) approach (Neuenschwander et al., 2010; Schmidli et al., 2014). Suppose that there are two endpoints ($I = 2$) to be evaluated in a randomized clinical trial comparing a treatment versus placebo with equal sample size $n_0^{(c)} = n_0^{(t)} = 150$. The control information is also available in $J = 6$ historical studies with sample sizes 100, 100, 200, 200, 300, and 300, with the response rates 0.4 and 0.3 for the two endpoints. We consider FWER to be controlled at $\alpha = 0.05$.

We consider historical control data as in Table 1. The number of responders $R_{i,j}^{(c)}$ for endpoint i , $i = 1, 2$, study j , $j = 1, \dots, 6$ is simulated from a Binomial distribution with rate 0.4 for endpoint $i = 1$ and 0.3 for endpoint $i = 2$. The empirical correlation of estimated response rate $R_{i,j}^{(c)}/n_j^{(c)}$ between two endpoints is 0.01. Additional simulation studies with an empirical correlation around 0.5 are conducted in the Supplemental Materials and demonstrate consistent findings.

j	1	2	3	4	5	6
$n_j^{(c)}$	100	100	200	200	300	300
$R_{1,j}^{(c)}$	33	41	78	81	115	113
$R_{2,j}^{(c)}$	31	28	69	68	94	97

Table 1: Control data from $J = 6$ historical studies.

To implement our DNN-based method, we first approximate the posterior probability \mathbf{S} in (3) based on Algorithm 1 with training data size $B = 8,000$. Its training input data $\mathbf{M} = \{R_{1,0}^{(c)}, R_{2,0}^{(c)}, R_{1,0}^{(t)}, R_{2,0}^{(t)}\}$ are drawn from Binomial distributions with rates $\{\psi_{1,0}^{(c)}, \psi_{2,0}^{(c)}, \psi_{1,0}^{(t)}, \psi_{2,0}^{(t)}\}$, which are further simulated from the following 4 patterns with equal size $B/4 = 2,000$,

1. $\psi_{1,0}^{(c)} \sim \text{Unif}(0.2, 0.7)$; $\psi_{2,0}^{(c)} \sim \text{Unif}(0.1, 0.6)$; $\Delta_{1,0} = 0$; $\Delta_{2,0} = 0$,
2. $\psi_{1,0}^{(c)} \sim \text{Unif}(0.2, 0.7)$; $\psi_{2,0}^{(c)} \sim \text{Unif}(0.1, 0.6)$; $\Delta_{1,0} \sim \text{Unif}(-0.1, 0.2)$; $\Delta_{2,0} = 0$,
3. $\psi_{1,0}^{(c)} \sim \text{Unif}(0.2, 0.7)$; $\psi_{2,0}^{(c)} \sim \text{Unif}(0.1, 0.6)$; $\Delta_{1,0} = 0$; $\Delta_{2,0} \sim \text{Unif}(-0.1, 0.2)$,
4. $\psi_{1,0}^{(c)} \sim \text{Unif}(0.2, 0.7)$; $\psi_{2,0}^{(c)} \sim \text{Unif}(0.1, 0.6)$; $\Delta_{1,0} \sim \text{Unif}(-0.1, 0.2)$; $\Delta_{2,0} \sim \text{Unif}(-0.1, 0.2)$,

where Unif denotes the Uniform distribution, and the treatment response rates are calculated at $\psi_{i,0}^{(t)} = \psi_{i,0}^{(c)} + \Delta_{i,0}$ for $i = 1, 2$. The ranges of above Uniform distributions are determined based on previous knowledge that $\psi_{1,0}^{(c)}$ is between 0.2 and 0.7, while $\psi_{2,0}^{(c)}$ is within 0.1 and 0.6. The Uniform distribution can be substituted by other sampling distributions, e.g., flat normal distribution. For this simulation study, the training data size $B = 8,000$ is sufficient to give DNN satisfactory performance, for example training MSE less than 10^{-3} . It can be increased to accommodate more distinct training features, as in the next section of case study.

Next we obtain posterior samples of $\psi_{i,0}^{(c)}$ from model (2) based on the Markov chain Monte Carlo (MCMC) method implemented by the R package `R2jags` (Su and Yajima, 2015). We put a vague prior on θ following a Normal distribution with mean zero and precision 0.01, and an InverseWishart(Σ_0, k) prior for Σ with Σ_0 as a unit diagonal matrix and $k = I + 1$. The convergence of the MCMC algorithm is checked by the criteria of $\widehat{R} < 1.01$ among 3 chains, where \widehat{R} is the ratio of between-chain versus within-chain variability (Gelman et al., 1992; Berry et al., 2010). The posterior distribution of $\psi_{i,0}^{(t)}$ is a Beta distribution with a non-informative Beta prior $a_i = b_i = 1$ based on the Beta-Binomial conjugate model in (1). Our posterior probability S_i in (3) is evaluated by 30,000 posterior samples with $\theta_i = 0$. In Step 2 of selecting a proper DNN structure, we consider a pool of four candidate structures: $H_l = 2$ hidden layers with $H_n = 40$ nodes per layer, $H_l = 2$ and $H_n = 60$, $H_l = 3$ and $H_n = 40$, $H_l = 3$ and $H_n = 60$. The batch size H_b is 100, and the number of training epochs H_e is 1,000 with dropout rate $H_d = 0.1$. The above parameters are used throughout this article unless specified otherwise. In this simulation study, we choose a DNN structure with $H_l = 2$ hidden layers, $H_n = 60$ nodes per layer with the smallest validation MSE among four candidates. This DNN structure is utilized in Algorithm 2 as well. From the final fitting at Step 3, we obtain DNN $\widehat{\mathbf{S}} = F_S(\mathbf{M}; \widehat{\phi})$ to estimate \mathbf{S} in (3).

In Algorithm 2 of approximating the critical values, we simulate $B_1 = B_2 = B_{12} = 2,000$ datasets to reflect patterns of H_1 in (4), H_2 in (5) and H_{12} in (6),

1. $\psi_{1,0}^{(c,t)} \sim \text{Unif}(0.2, 0.7)$; $\psi_{2,0}^{(c)} \sim \text{Unif}(0.1, 0.6)$; $\Delta_{2,0} \sim \text{Unif}(-0.1, 0.2)$; $\psi_{2,0}^{(t)} = \psi_{2,0}^{(c)} + \Delta_{2,0}$,
2. $\psi_{1,0}^{(c)} \sim \text{Unif}(0.2, 0.7)$; $\Delta_{1,0} \sim \text{Unif}(-0.1, 0.2)$; $\psi_{1,0}^{(t)} = \psi_{1,0}^{(c)} + \Delta_{1,0}$; $\psi_{2,0}^{(c,t)} \sim \text{Unif}(0.1, 0.6)$,
3. $\psi_{1,0}^{(c,t)} \sim \text{Unif}(0.2, 0.7)$; $\psi_{2,0}^{(c,t)} \sim \text{Unif}(0.1, 0.6)$.

The number of iterations of calculating critical values are $B'_1 = B'_2 = B'_{12} = 100,000$.

We implement the Meta-Analytic-Predictive (MAP) priors (Neuenschwander et al., 2010) and two robust MAP priors with a weight of $w = 50\%$ and $w = 80\%$ non-informative component (Schmidli et al., 2014) by the R package **RBesT** (Weber, 2020). These methods handle data from each endpoint separately, instead of modeling them jointly as in our model (2). The setup follows their default settings with a weakly informative Half-Normal $(0, 1)$ prior on the standard deviation of the logit of the response rate (Weber et al., 2019). Hypothesis testing is also based on posterior probabilities S_i , but the constant critical values \tilde{c} are chosen by a grid search method to control testing type I error rates not exceeding $\alpha = 0.05$ within a certain range of null response rates in the following Table 2.

In Table 2, we first evaluate the error rates of falsely rejecting H_{12} , H_1 or H_2 under the global null hypothesis where $\Delta_{1,0} = \Delta_{2,0} = 0$. The number of iterations in testing is 100,000. Our proposed method has relatively accurate control on three error rates at $\alpha = 0.05$ across three scenarios with varying $\psi_{1,0}^{(c)}$ and $\psi_{2,0}^{(c)}$. For MAP and two robust MAPs, we choose their constant critical values \tilde{c} 's (introduced in Section 2) at 0.9977, 0.9927, and 0.9867, respectively, by the grid search method such that the probability of rejecting H_{12} reaches the nominal level of 0.05 under the “worst case scenario” with $\psi_{1,0}^{(c)} = 0.5$ and $\psi_{2,0}^{(c)} = 0.4$. This scenario has the largest type I error rate given the same critical value under the null space evaluated in Table 2. This simulation-based type I error rate control ensures that FWER does not exceed α under all three null cases, but leads to conservative error rates and potential power loss in some cases as evaluated later. The critical value $\tilde{c} = 0.9977$ of MAP is interpreted as a cutoff to claim a significant treatment effect based on endpoint i , because we reject the null hypothesis pertaining to endpoint i if its posterior probability S_i in (3) is larger than \tilde{c} based on Section 2.

Under a single null hypothesis where only a single Δ_i is equal to zero, the error rate happens when this particular true null hypothesis is erroneously rejected. All methods control this error rate well below α . When it comes to alternative hypotheses, our method has a much higher power of rejecting each elementary null hypothesis, and a higher power of rejecting at least one of them than MAP and two RMAPs under $\psi_{1,0}^{(c)} = 0.3, \psi_{2,0}^{(c)} = 0.2$ and $\psi_{1,0}^{(c)} = 0.4, \psi_{2,0}^{(c)} = 0.3$. This is mainly due to the conservative type I error of using a constant critical value for MAP and RMAPs. When response rates are higher at $\psi_{1,0}^{(c)} = 0.5, \psi_{2,0}^{(c)} = 0.4$, MAP usually has the best power performance, followed by

our DNN method, and then two RMAPs. Note that there are two scenarios with prior-data conflict given that historical control rates are 0.4, 0.3 for the first and the second endpoint, respectively.

Table 3 presents the bias and Table 4 shows the root of mean squared error (RMSE) of posterior means of $\psi_{1,0}^{(c)}$ and $\psi_{2,0}^{(c)}$. In scenarios where the current control rates and historical rates are consistent at 0.4 for the first endpoint and 0.3 for the second endpoint, all methods have small biases, and MAP has the smallest RMSE. Under cases with prior-data conflict, DNN and two RMAPs have better bias than MAP, and moreover DNN has the smallest RMSE. The overall conclusion is that our DNN-based method enjoys the robustness of RMAP under prior-data conflict, and preserves power by modeling critical values as compared with MAP and RMAP by using constant critical values.

Figure 3 shows the approximation errors of DNN in estimating posterior means of $\psi_{1,0}^{(c)}$ and $\psi_{2,0}^{(c)}$, and posterior probabilities S_1 and S_2 in (3) from $B = 8,000$ training data. The MSE from DNN training is approximately 0.001. Errors are relatively larger in approximating S_1 and S_2 from (3), because their training labels have more randomness in the Monte Carlo estimates as compared with the empirical posterior means of $\psi_{1,0}^{(c)}$ and $\psi_{2,0}^{(c)}$.

$\psi_{1,0}^{(c)}$	$\psi_{2,0}^{(c)}$	$\Delta_{1,0}$	$\Delta_{2,0}$	DNN			MAP			RMAP with $w = 50\%$			RMAP with $w = 80\%$		
				H_{12}	H_1	H_2	H_{12}	H_1	H_2	H_{12}	H_1	H_2	H_{12}	H_1	H_2
Global null hypothesis															
<u>0.3</u>	<u>0.2</u>	0	0	4.9%	3.0%	1.9%	<0.1%	<0.1%	<0.1%	0.9%	0.3%	0.6%	2.1%	0.9%	1.2%
0.4	0.3			4.9%	3.2%	1.8%	0.3%	0.2%	<0.1%	0.9%	0.7%	0.2%	1.9%	1.2%	0.7%
<u>0.5</u>	<u>0.4</u>			4.8%	3.7%	1.2%	4.8%	2.6%	2.3%	5.1%	2.4%	2.7%	5.0%	2.3%	2.7%
Single null hypothesis															
0.4	0.3	0.1	0.1	49.3%	48.3%	1.9%	29.4%	29.4%	<0.1%	37.7%	37.6%	0.2%	40.8%	40.4%	0.7%
		0	0.1	42.2%	2.5%	40.9%	16.2%	0.2%	16.0%	28.1%	0.7%	27.5%	36.6%	1.2%	35.8%
Alternative hypothesis															
<u>0.3</u>	<u>0.2</u>	0.1	0.1	71.8%	45.1%	47.9%	6.3%	3.0%	3.4%	30.9%	13.0%	20.6%	50.6%	24.8%	34.3%
		0.12	0.12	85.1%	58.6%	63.0%	13.6%	7.1%	6.9%	46.1%	22.3%	30.6%	67.0%	37.3%	47.3%
0.4	0.3	0.1	0.1	67.6%	44.3%	42.8%	41.1%	29.6%	16.2%	55.0%	37.9%	27.5%	61.5%	40.4%	35.4%
		0.12	0.12	81.3%	57.7%	57.5%	62.6%	46.3%	30.5%	74.3%	53.6%	44.5%	78.6%	55.1%	52.2%
<u>0.5</u>	<u>0.4</u>	0.1	0.1	64.0%	45.1%	37.0%	68.0%	42.0%	44.8%	59.1%	32.6%	39.2%	60.7%	35.5%	39.1%
		0.12	0.12	78.6%	58.1%	52.6%	83.3%	57.4%	60.9%	72.6%	44.1%	50.9%	75.0%	48.5%	51.5%

Note: underlined scenarios are with prior-data conflict where historical control rates are 0.4, 0.3 for the first and the second endpoint, respectively.

Table 2: Type I error rate and power of DNN-based approach, MAP and RMAP.

$\psi_{1,0}^{(c)}$	$\psi_{2,0}^{(c)}$	$\Delta_{1,0}$	$\Delta_{2,0}$	DNN		MAP		RMAP with $w = 50\%$		RMAP with $w = 80\%$	
				$\psi_{1,0}^{(c)}$	$\psi_{2,0}^{(c)}$	$\psi_{1,0}^{(c)}$	$\psi_{2,0}^{(c)}$	$\psi_{1,0}^{(c)}$	$\psi_{2,0}^{(c)}$	$\psi_{1,0}^{(c)}$	$\psi_{2,0}^{(c)}$
Global null hypothesis											
<u>0.3</u>	<u>0.2</u>	0	0	0.025	0.029	0.048	0.050	0.027	0.018	0.015	0.010
0.4	0.3			0.004	0.006	-0.010	0.015	-0.007	0.012	-0.004	0.008
<u>0.5</u>	<u>0.4</u>			-0.015	-0.016	-0.050	-0.046	-0.020	-0.024	-0.009	-0.012
Single null hypothesis											
0.4	0.3	0.1	0	0.004	0.006	-0.011	0.015	-0.008	0.012	-0.004	0.008
		0	0.1	0.004	0.006	-0.011	0.014	-0.008	0.011	-0.004	0.008
Alternative hypothesis											
<u>0.3</u>	<u>0.2</u>	0.1	0.1	0.025	0.029	0.046	0.049	0.026	0.018	0.015	0.010
		0.12	0.12	0.025	0.029	0.048	0.048	0.026	0.018	0.014	0.010
0.4	0.3	0.1	0.1	0.004	0.006	-0.011	0.015	-0.008	0.012	-0.004	0.008
		0.12	0.12	0.004	0.006	-0.010	0.015	-0.007	0.012	-0.004	0.008
<u>0.5</u>	<u>0.4</u>	0.1	0.1	-0.015	-0.016	-0.052	-0.043	-0.020	-0.024	-0.009	-0.012
		0.12	0.12	-0.015	-0.016	-0.054	-0.044	-0.021	-0.024	-0.009	-0.012

Note: underlined scenarios are with prior-data conflict where historical control rates are 0.4, 0.3 for the first and the second endpoint, respectively.

Table 3: Bias of posterior means $\psi_{1,0}^{(c)}$ and $\psi_{2,0}^{(c)}$ in DNN, MAP and RMAP.

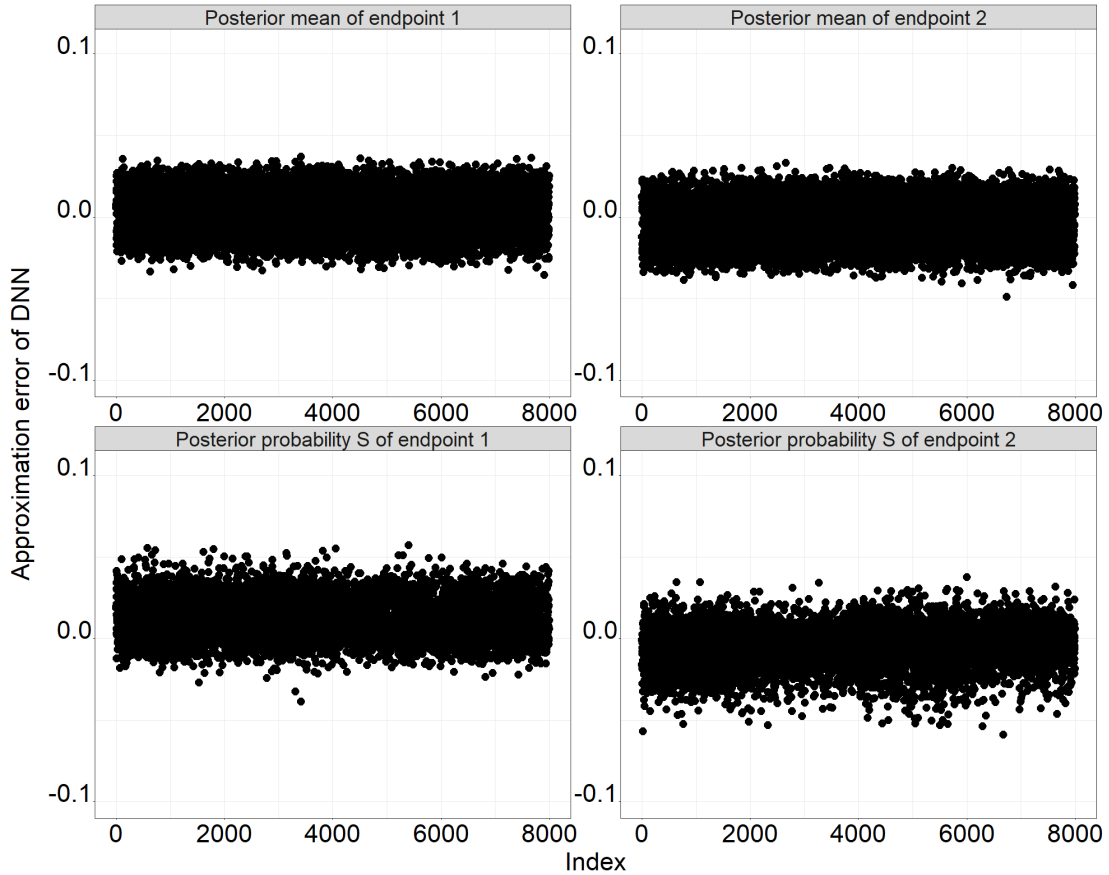


Figure 3: Approximation error of DNN in estimating posterior means of $\psi_{1,0}^{(c)}$ and $\psi_{2,0}^{(c)}$, and posterior probabilities S_1 and S_2 in (3).

$\psi_{1,0}^{(c)}$	$\psi_{2,0}^{(c)}$	$\Delta_{1,0}$	$\Delta_{2,0}$	DNN		MAP		RMAP with $w = 50\%$		RMAP with $w = 80\%$	
				$\psi_{1,0}^{(c)}$	$\psi_{2,0}^{(c)}$	$\psi_{1,0}^{(c)}$	$\psi_{2,0}^{(c)}$	$\psi_{1,0}^{(c)}$	$\psi_{2,0}^{(c)}$	$\psi_{1,0}^{(c)}$	$\psi_{2,0}^{(c)}$
Global null hypothesis											
<u>0.3</u>	<u>0.2</u>	0	0	0.039	0.039	0.055	0.061	0.048	0.046	0.043	0.038
0.4	0.3			0.031	0.029	0.018	0.020	0.023	0.024	0.029	0.029
<u>0.5</u>	<u>0.4</u>			0.037	0.036	0.064	0.052	0.054	0.048	0.047	0.044
Single null hypothesis											
0.4	0.3	0.1	0	0.031	0.029	0.018	0.020	0.024	0.024	0.030	0.029
		0	0.1	0.031	0.029	0.018	0.020	0.023	0.024	0.030	0.029
Alternative hypothesis											
<u>0.3</u>	<u>0.2</u>	0.1	0.1	0.039	0.039	0.053	0.062	0.048	0.046	0.043	0.038
		0.12	0.12	0.039	0.039	0.054	0.060	0.048	0.045	0.043	0.038
0.4	0.3	0.1	0.1	0.031	0.029	0.018	0.020	0.024	0.024	0.030	0.029
		0.12	0.12	0.031	0.029	0.018	0.020	0.023	0.024	0.029	0.028
<u>0.5</u>	<u>0.4</u>	0.1	0.1	0.037	0.036	0.066	0.052	0.054	0.048	0.047	0.044
		0.12	0.12	0.037	0.036	0.065	0.051	0.054	0.047	0.047	0.044

Note: underlined scenarios are with prior-data conflict where historical control rates are 0.4, 0.3 for the first and the second endpoint, respectively.

Table 4: RMSE of posterior means $\psi_{1,0}^{(c)}$ and $\psi_{2,0}^{(c)}$ in DNN, MAP and RMAP.

5 A case study

We design a generic randomized clinical trial evaluating the efficacy of a study drug versus an active comparator secukinumab 300 mg (Langley et al., 2014) in patients with moderate-to-severe plaque psoriasis with equal sample size per group $n_0^{(c)} = n_0^{(t)} = 200$. We consider the co-primary endpoints in Langley et al. (2014): the proportion of patients achieving a reduction of 75% or more from baseline in the Psoriasis Area-and-Severity Index score (PASI 75) and the proportion of patients achieving a score of 0 (clear) or 1 (almost clear) on a 5-point modified investigator’s global assessment (MIGA 0/1) at week 12. The control information is available in $J = 3$ historical studies: ERASURE, FIXTURE (Langley et al., 2014) and JUNCTURE (Paul et al., 2015) with data summarized in Table 5. The weighted observed response rates are approximately 0.80 and 0.65 for PASI 75 and MIGA 0/1, respectively. We evaluate the performance of different methods on the following three scenarios on response rates from the current trial:

1. Prior-data conflict scenario 1 (S1): $\psi_{1,0}^{(c)} = 0.7$ and $\psi_{2,0}^{(c)} = 0.55$,

2. Prior-data conflict scenario 2 (S2): $\psi_{1,0}^{(c)} = 0.9$ and $\psi_{2,0}^{(c)} = 0.75$,
3. Prior-data consistent scenario (S3): $\psi_{1,0}^{(c)} = 0.8$ and $\psi_{2,0}^{(c)} = 0.65$.

Historical study	ERASURE	FIXTURE	JUNCTURE	Total
$n_j^{(c)}$	245	323	60	628
$R_{1,j}^{(c)}$ (rate) of PASI 75	200 (0.82)	249 (0.77)	52 (0.87)	501 (0.80)
$R_{2,j}^{(c)}$ (rate) of MIGA 0/1	160 (0.65)	202 (0.63)	44 (0.73)	406 (0.65)

Table 5: Data of the active comparator secukinumab 300 mg in $J = 3$ historical studies.

When generating training data in our method, we consider the range of $\psi_{1,0}^{(c)}$ as 0.65 to 0.95, the range of $\psi_{2,0}^{(c)}$ as 0.5 to 0.8, and the ranges of $\Delta_{1,0}$ and $\Delta_{2,0}$ as -0.1 to 0.1 . The choices of above ranges are based on the team’s knowledge, such as the historical data in Table 5, target product profile (TPP) of the new drug, et cetera. These ranges can be set wider as needed. As compared with simulation studies in Section 4, we increase the training data size B in Algorithm 1 from 8,000 to 16,000 to get DNN training MSE less than 10^{-3} . This is to accommodate a larger number of distinct features from training input data \mathbf{M} due to larger current sample sizes $n_0^{(c)}$ and $n_0^{(t)}$. The constant critical values in MAP, RMAP with $w = 50\%$, and RMAP with $w = 80\%$ are 0.987, 0.984, and 0.980, respectively, to protect maximum testing type I error rates not exceeding $\alpha = 0.05$ under three scenarios S1, S2, and S3. The computation of constant critical values of MAP and RMAP is discussed in Section 4. The selected DNN has $H_l = 2$ hidden layers and $H_n = 60$ nodes per layer. Other parameter setups are the same as Section 4.

Similar to what we observe on type I error rates in Table 2, MAP and two RMAPs have conservative type I error rates under scenarios with lower response rates (i.e., S1 and S3). In terms of power, our DNN-based method generally has a higher probability of rejecting at least one null hypothesis (Figure 4a), rejecting the first null hypothesis (Figure 4b), and rejecting the second null hypothesis (Figure 4c) than MAP and two RMAPs under S1 and S3. Our method preserves power in these cases by modeling critical values in Algorithm 2. Under S2 where all methods have type I error rates of approximately 5%, all methods have similar power performance. The RMAP methods demonstrate the smallest absolute bias for the posterior means $\psi_{1,0}^{(c)}$ (Figure 5a) and $\psi_{2,0}^{(c)}$ (Figure 5b) in general. Our DNN approach has smaller bias than MAP under scenarios S1 and S2 with prior-data conflict.

The RMSE of our method is the smallest under two prior-data conflict scenarios, but is slightly larger than comparators under the prior-data consistent scenario (Figure 6a, 6b). Therefore, our proposed method has satisfactory RMSE under prior-data conflicts, and preserves power by estimating critical values with DNN.

6 Concluding remarks

In this article, we construct a prospective DNN-based framework from the Bayesian hierarchical model to synthesize control information from multiple endpoints. Our two-stage method first approximates posterior probabilities and then estimates critical values. The decision functions for hypothesis testing based on DNN training can be locked in files before initiation of the current trial to ensure study integrity, which is appealing to regulatory agencies.

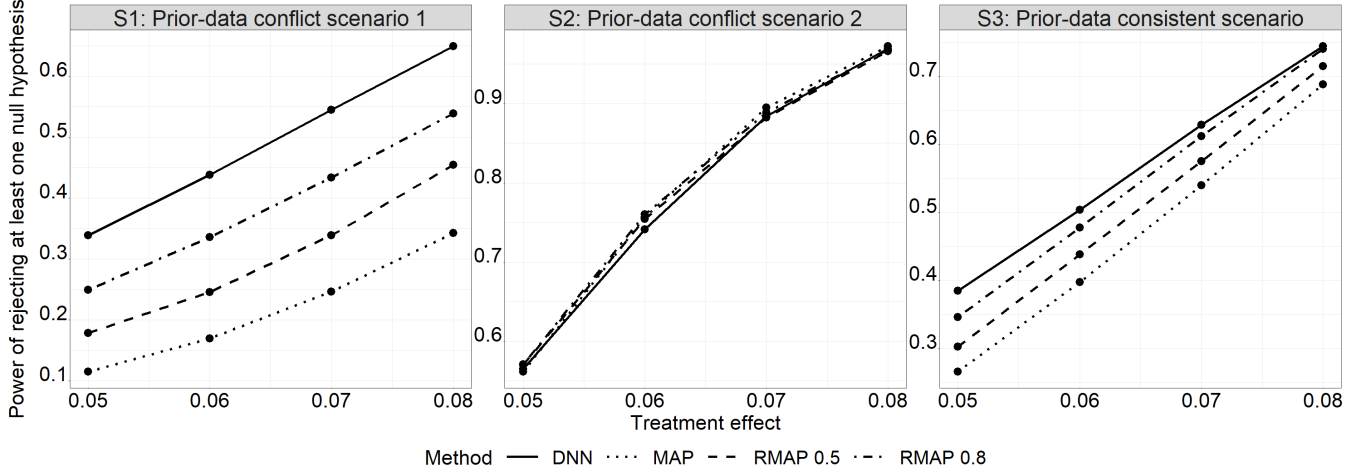
Our DNN-based prospective algorithm can also save computational time as compared with the traditional simulation method. Taking the case study in Section 5 for illustration, there are 12 setups (4 magnitudes of treatment effect \times 3 scenarios) in total and 100,000 testing iterations per setup. As shown in Table 6, it takes approximately 34 hours for DNN to conduct the computation, while over 700 hours for the traditional method. The main saving is due to the fact that DNN builds an approximating function in Algorithm 1 with only $B = 16,000$ rounds of MCMC computation required. The final testing is fast based on well-trained DNNs. On the contrary, the traditional approach needs to perform MCMC for every iteration (1,200,000 in total) in testing.

Method	Algorithm 1	Algorithm 2	Testing	Total time
DNN	11.89	22.08	0.04	34.01
Traditional Simulation	-	-	> 700	> 700

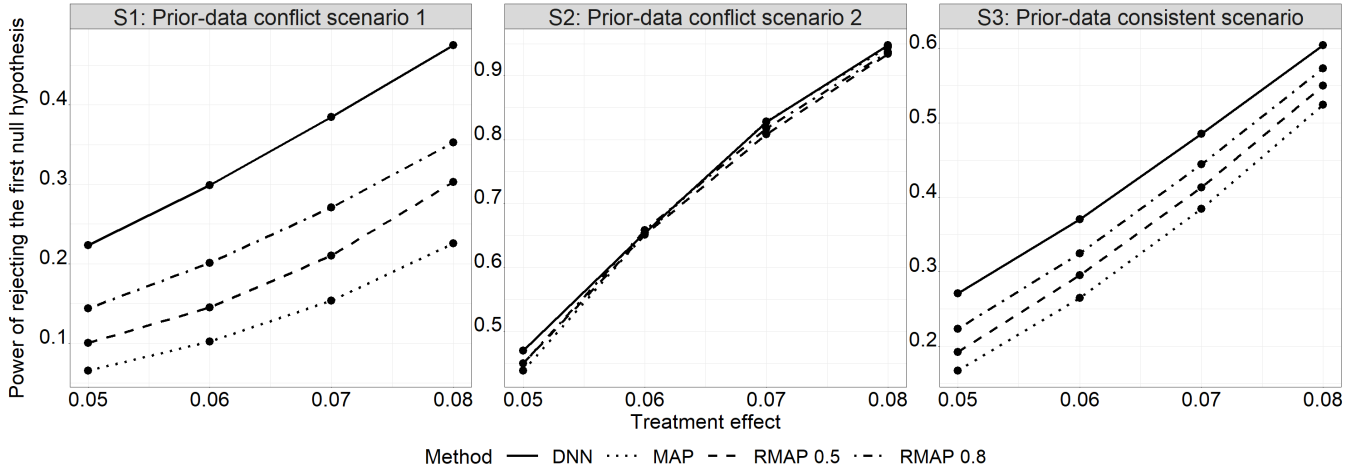
Table 6: Computational time (in hours) of DNN and MCMC in the case study.

Another important contribution of our work is to model the critical values by DNN to control FWER. A common practice is to choose the cutoff value by a grid-search method to control type I errors in testing within a certain range of the null space. Simulations show a moderate power gain of our proposed method, especially when the constant critical value has a conservative error rate. To accommodate approximation errors, a smaller working significance level can be utilized to control

(a) Power of rejecting at least one null hypothesis.



(b) Power of rejecting the first null hypothesis.



(c) Power of rejecting the second null hypothesis.

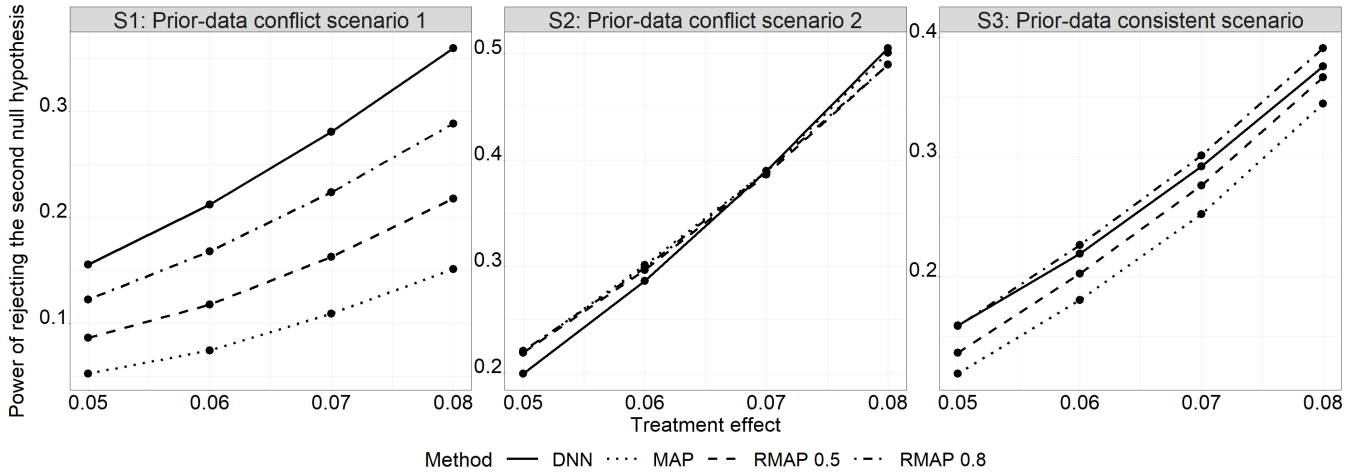
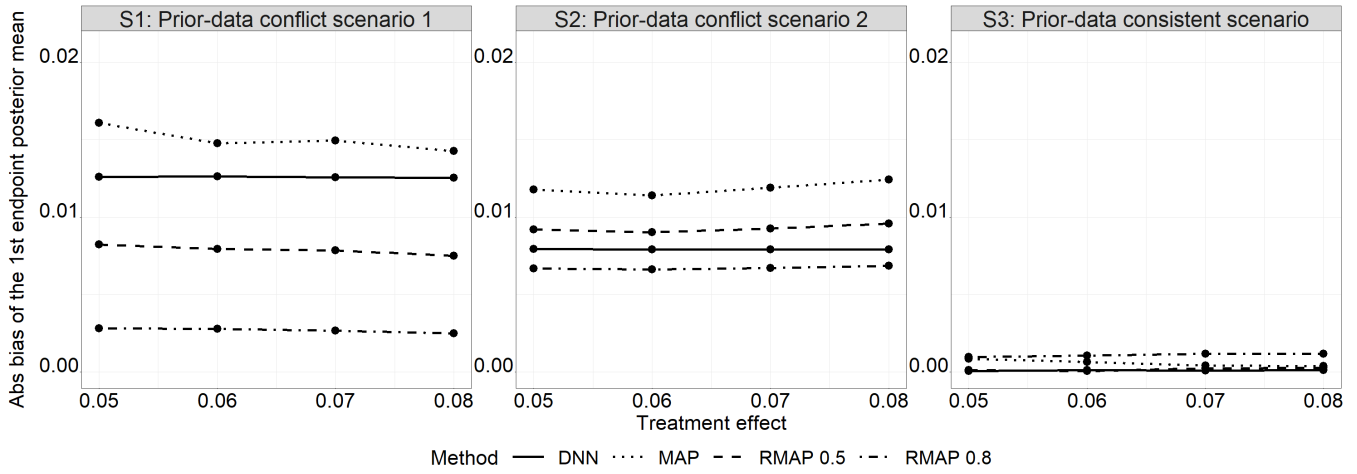


Figure 4: Power performance of DNN, MAP and two RMAPs.

(a) Absolute bias of the posterior mean $\psi_{1,0}^{(c)}$.



(b) Absolute bias of the posterior mean $\psi_{2,0}^{(c)}$.

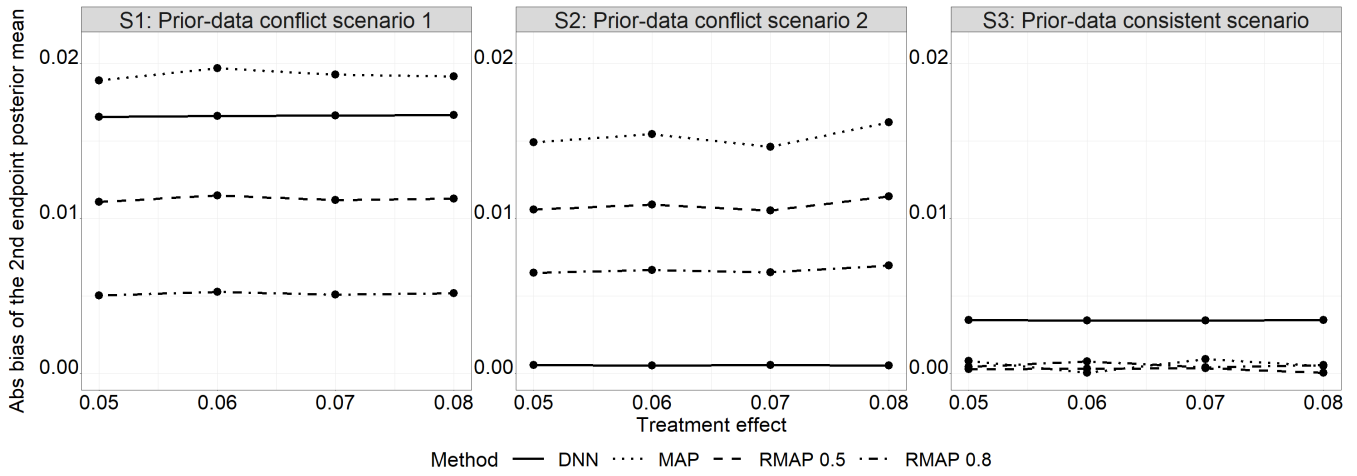
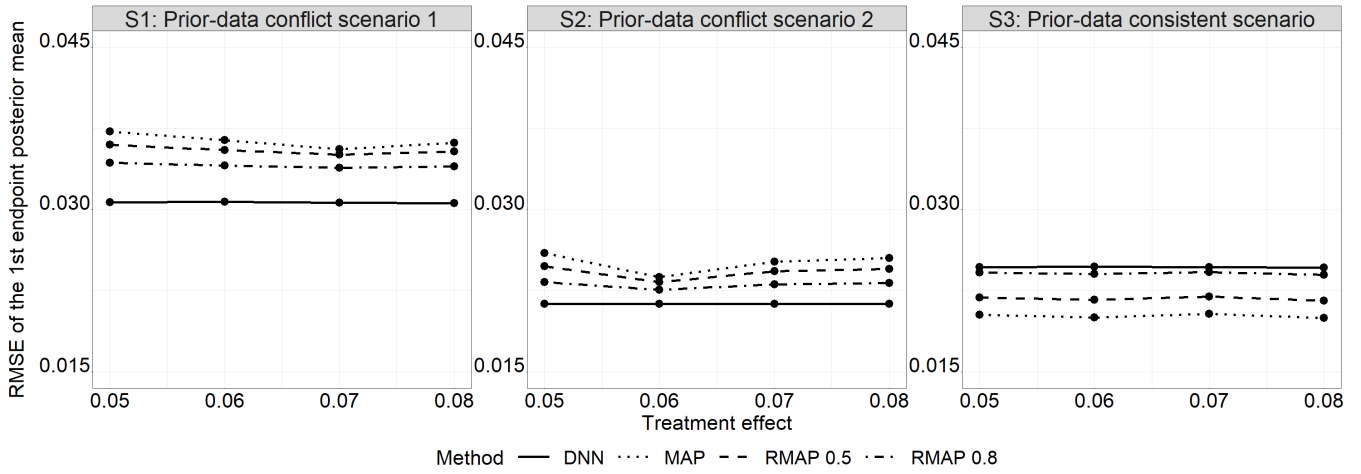


Figure 5: Absolute bias of posterior means $\psi_{1,0}^{(c)}$ and $\psi_{2,0}^{(c)}$ in DNN, MAP and two RMAPs.

(a) RMSE of the posterior mean $\psi_{1,0}^{(c)}$.



(b) RMSE of the posterior mean $\psi_{2,0}^{(c)}$.

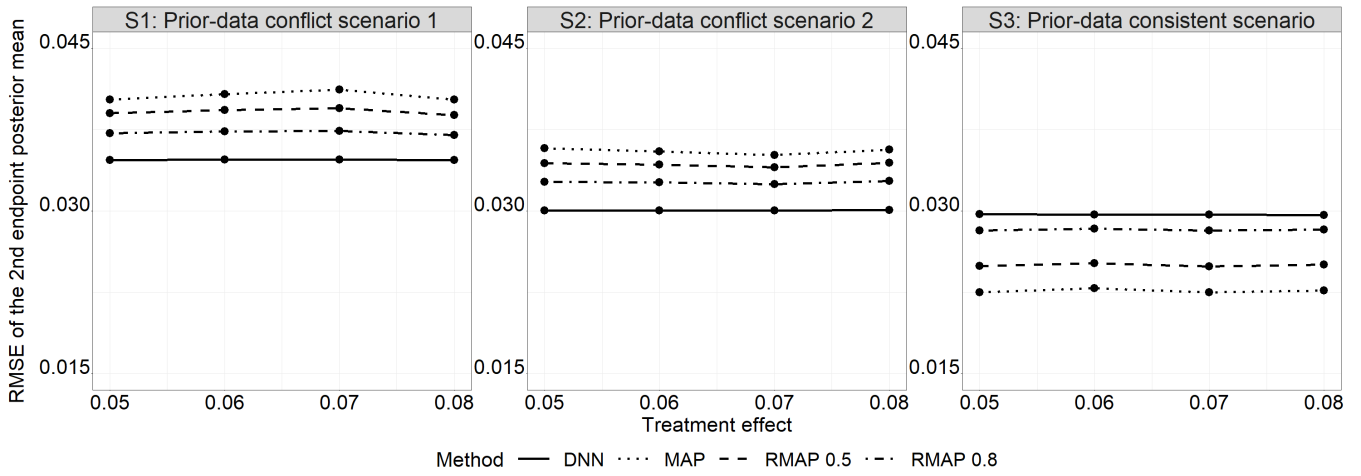


Figure 6: RMSE of posterior means $\psi_{1,0}^{(c)}$ and $\psi_{2,0}^{(c)}$ in DNN, MAP and two RMAPs.

validated type I error rates strictly smaller than the nominal level, if necessary. Our framework can be broadly generalized to other types of Bayesian designs when the critical value is not available analytically in finite samples.

We discuss some potential limitations of the proposed method. Firstly, there is a lack of theoretical understanding of the upper bound of the approximation error when estimating posterior probabilities \mathbf{S} by DNN in Algorithm 1, and estimating critical values by DNN in Algorithm 2. In this article, we provide empirical evidence to address this by checking model fitting MSE and the error plot in Figure 3. Moreover, our method requires a few more hours in simulating training data for DNNs before the current trial conduct, as shown in Table 6. However, after observing current trial data, we can instantly compute the posterior probabilities and critical values to conduct hypothesis testing. Table 6 shows that our method saves considerable computational time compared to the traditional simulation method in the testing stage.

Supplemental Materials

Supplemental Materials include additional simulation results of Section 4 with an empirical correlation at 0.5. The R code is available at https://github.com/tian-yu-zhan/Deep_Historical_Borrowing.

7 Acknowledgements

This manuscript was sponsored by AbbVie, Inc. AbbVie contributed to the design, research, and interpretation of data, writing, reviewing, and approving the content. Tianyu Zhan, Ziqian Geng, Yihua Gu, Li Wang and Xiaohong Huang are employees of AbbVie Inc. Yiwang Zhou was a 2020 summer intern at AbbVie Inc. Jian Kang is Professor at Department of Biostatistics, University of Michigan, Ann Arbor. Professor Kang’s research was partially supported by NIH R01 GM124061 and R01 MH105561. Elizabeth H. Slate is Distinguished Research Professor, Duncan McLean and Pearl Levine Fairweather Professor at Department of Statistics, Florida State University. This work was initiated when Professor Slate was the AbbVie Visiting Scholar in Honor of David C. Jordan

from 2018 to 2019. All authors may own AbbVie stock.

Authors would also like to thank the editor Margaret Gamalo, an anonymous associate editor and three anonymous reviewers for their constructive comments.

References

- Bach, F. (2017). Breaking the curse of dimensionality with convex neural networks. *The Journal of Machine Learning Research*, 18(1):629–681.
- Berry, S. M., Carlin, B. P., Lee, J. J., and Muller, P. (2010). *Bayesian adaptive methods for clinical trials*. CRC press.
- Bretz, F., Hothorn, T., and Westfall, P. (2016). *Multiple comparisons using R*. CRC Press.
- Chollet, F. and Allaire, J. J. (2018). *Deep Learning with R*. Manning Publications Co., Greenwich, CT, USA.
- Chow, S.-C., Wang, H., and Shao, J. (2007). *Sample size calculations in clinical research*. CRC press.
- Food and Drug Administration (2017). Multiple endpoints in clinical trials guidance for industry. <https://www.fda.gov/downloads/drugs/guidancecomplianceregulatoryinformation/guidances/ucm536750.pdf>.
- Gelman, A., Rubin, D. B., et al. (1992). Inference from iterative simulation using multiple sequences. *Statistical Science*, 7(4):457–472.
- Goodfellow, I., Bengio, Y., and Courville, A. (2016). *Deep learning*. MIT press.
- Graf, A. C., Bauer, P., Glimm, E., and Koenig, F. (2014). Maximum type 1 error rate inflation in multiarmed clinical trials with adaptive interim sample size modifications. *Biometrical Journal*, 56(4):614–630.
- Hinton, G., Srivastava, N., and Swersky, K. (2012). Neural networks for machine learning. *Coursera, video lectures*, 307.

- Langley, R. G., Elewski, B. E., Lebwohl, M., Reich, K., Griffiths, C. E., Papp, K., Puig, L., Nakagawa, H., Spelman, L., Sigurgeirsson, B., et al. (2014). Secukinumab in plaque psoriasis—results of two phase 3 trials. *New England Journal of Medicine*, 371(4):326–338.
- Neuenschwander, B., Capkun-Niggli, G., Branson, M., and Spiegelhalter, D. J. (2010). Summarizing historical information on controls in clinical trials. *Clinical Trials*, 7(1):5–18.
- Paul, C., Lacour, J.-P., Tedremets, L., Kreutzer, K., Jazayeri, S., Adams, S., Guindon, C., You, R., Papavassilis, C., and Group, J. S. (2015). Efficacy, safety and usability of secukinumab administration by autoinjector/pen in psoriasis: a randomized, controlled trial (junction). *Journal of the European Academy of Dermatology and Venereology*, 29(6):1082–1090.
- Proschan, M. A. and Hunsberger, S. A. (1995). Designed extension of studies based on conditional power. *Biometrics*, pages 1315–1324.
- Schmidli, H., Gsteiger, S., Roychoudhury, S., O’Hagan, A., Spiegelhalter, D., and Neuenschwander, B. (2014). Robust meta-analytic-predictive priors in clinical trials with historical control information. *Biometrics*, 70(4):1023–1032.
- Su, Y.-S. and Yajima, M. (2015). *R2jags: Using R to Run ‘JAGS’*. R package version 0.5-7.
- Tamhane, A. C. and Gou, J. (2018). Advances in p-value based multiple test procedures. *Journal of Biopharmaceutical Statistics*, 28(1):10–27.
- Viele, K., Berry, S., Neuenschwander, B., Amzal, B., Chen, F., Enas, N., Hobbs, B., Ibrahim, J. G., Kinnersley, N., Lindborg, S., et al. (2014). Use of historical control data for assessing treatment effects in clinical trials. *Pharmaceutical Statistics*, 13(1):41–54.
- Weber, S. (2020). *RBesT: R Bayesian Evidence Synthesis Tools*. R package version 1.6-0.
- Weber, S., Li, Y., Seaman, J., Kakizume, T., and Schmidli, H. (2019). Applying meta-analytic predictive priors with the R Bayesian evidence synthesis tools. *arXiv preprint arXiv:1907.00603*.
- Yarotsky, D. (2017). Error bounds for approximations with deep ReLU networks. *Neural Networks*, 94:103–114.

Zhan, T., Hartford, A., Kang, J., and Offen, W. (2020a). Optimizing graphical procedures for multiplicity control in a confirmatory clinical trial via deep learning. *Statistics in Biopharmaceutical Research*, pages 1–11.

Zhan, T., Zhang, H., Hartford, A., and Mukhopadhyay, S. (2020b). Modified goldilocks design with strict type I error control in confirmatory clinical trials. *Journal of Biopharmaceutical Statistics*, 30(5):821–833.